

Magnetic reconnection between a solar filament and nearby coronal loops

Leping Li^{1*}, Jun Zhang¹, Hardi Peter², Eric Priest³, Huadong Chen¹, Lijia Guo², Feng Chen² and Duncan Mackay³

Magnetic reconnection^{1,2} is difficult to observe directly but coronal structures on the Sun often betray the magnetic field geometry and its evolution³. Here we report the observation of magnetic reconnection between an erupting filament and its nearby coronal loops, resulting in changes in the filament connection. X-type structures form when the erupting filament encounters the loops. The filament becomes straight, and bright current sheets form at the interfaces. Plasmoids appear in these current sheets and propagate bi-directionally. The filament disconnects from the current sheets, which gradually disperse and disappear, then reconnects to the loops. This evolution suggests successive magnetic reconnection events predicted by theory¹ but rarely detected with such clarity in observations. Our results confirm the three-dimensional magnetic reconnection theory¹ and have implications for the evolution of dissipation regions and the release of magnetic energy for reconnection in many magnetized plasma systems.

Magnetic reconnection^{1,2} is considered to play an essential role in the rapid release of magnetic energy and its conversion to other forms⁴ (thermal, kinetic, and particle) in magnetized plasma systems throughout the universe (such as accretion disks, solar and stellar coronae, planetary magnetospheres, and laboratory plasmas). It shows the reconfiguration of the magnetic field geometry. In solar physics, numerous theoretical studies of magnetic reconnection^{5,6} have been undertaken to explain features such as flares and filament eruptions. In two-dimensional (2D) models, reconnection occurs at an X-point where anti-parallel magnetic field lines converge and reconnect^{1,5,6}. So far, many observations of magnetic reconnection signatures, for example, cusp-shaped post-flare loops⁷, loop-top hard X-ray sources^{3,8}, reconnection inflows^{3,9,10} and outflows^{3,10–12}, flare supra-arcades downflows^{13,14}, current sheets^{10,15}, and plasmoid ejections^{10,12}, have been reported by using remote sensing data. However, to directly observe the details of the magnetic reconnection process is difficult, because of the small spatial scale and the fast temporal evolution of the process.

A solar filament is a relatively cool and dense plasma structure in the corona suspended above a magnetic polarity inversion line, with ends rooted in regions with opposite magnetic polarity. Its spine, a narrow ribbon-like structure through the full filament, consists of horizontal and parallel threads when viewed from above¹⁶. In the region around a filament, the plasma beta, that is, the ratio of thermal to magnetic energy density, is below unity. Because of the high electrical conductivity, the magnetic flux is frozen into the coronal plasma¹³. The magnetic field topology is therefore often outlined by plasma trapped in the coronal magnetic

structures (such as filaments^{16,17} and coronal loops³). The change of these coronal structures hence suggests a change of magnetic topology³. Erupting filaments usually reconnect with ambient coronal structures, such as a coronal hole¹⁸, another filament¹⁹, or active region loops²⁰. However, the present observations give much greater detail of the reconnection process.

The Atmospheric Imaging Assembly²¹ (AIA) and Helioseismic and Magnetic Imager²² (HMI) onboard the Solar Dynamics Observatory²³ (SDO) provide full-disk multiwavelength images of the solar atmosphere and line-of-sight (LOS) magnetograms, with time cadences and spatial sampling of 12 s and 45 s, and 0.6''/pixel and 0.5''/pixel, respectively. On 1 January 2012, a quiet Sun filament, with a length of $720 \pm 5''$ and width of $13 \pm 1''$, was observed at around 00:00:20 UT by AIA 304 Å (showing plasma at ~ 0.05 MK) in the northern hemisphere (see Fig. 1a and Supplementary Fig. 1). To its east and south, two nearby filaments, marked by FE and FS in Fig. 1a (see also Supplementary Fig. 1), are observed. The filament was located above a polarity inversion line between opposite polarity magnetic field concentrations (see the yellow dotted line in Fig. 1c). Its northeastern endpoint roots in positive magnetic fields (see also Supplementary Fig. 6), whereas the southwestern endpoint roots in negative magnetic fields. The northeastern part of the filament is clearly identified in simultaneous AIA observations in channels imaging higher-temperature plasma, for example, 335 Å (~ 2.5 MK) and 211 Å (~ 1.9 MK). It shows up as an elongated dark structure, but the southwestern part is overlaid by dense closed loops (see Fig. 1b). To the southeast of the filament, a set of hot coronal loops L1 is present (see Fig. 1b), rooted in opposite magnetic polarities (see the green ellipses in Fig. 1b,c). This filament is also observed by the Extreme UltraViolet (UV) Imager (EUVI) onboard the Solar TERrestrial RELations Observatory²⁴ B (STEREO-B) under a different viewing angle (see Supplementary Fig. 2). It is located near the northwestern solar limb (see Supplementary Figs 1–3) in the field of view (FOV) of the EUVI, which supplies successive 304 Å (~ 0.05 MK) and 195 Å (~ 1.5 MK) images with spatial sampling and time cadences of 1.6''/pixel and 1.6''/pixel, and 10 min and 5 min, respectively.

Over the course of a little more than an hour, the whole structure of the filament underwent marked changes due to magnetic reconnection (see the blue and cyan dotted lines in Fig. 1c). These can be seen in the image sequence of Fig. 2, which shows the evolution of plasma at ~ 2.5 MK (335 Å; blue coloured) and ~ 0.9 MK (171 Å; orange coloured).

How does the magnetic reconnection happen? From about 00:10:00 UT, the northeastern part of the filament slowly rises

¹Key Laboratory of Solar Activity, National Astronomical Observatories, Chinese Academy of Sciences, Beijing 100012, China. ²Max-Planck Institute for Solar System Research (MPS), Göttingen 37077, Germany. ³School of Mathematics and Statistics, University of St Andrews, St Andrews, Fife KY16 9SS, UK. *e-mail: lepingli@nao.cas.cn

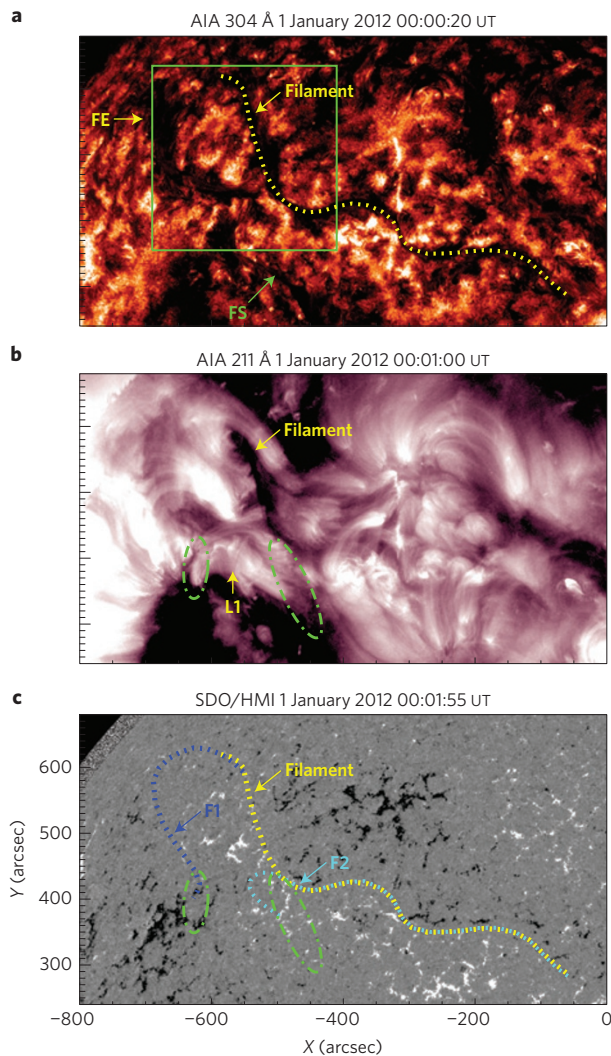


Figure 1 | SDO observations of a quiet Sun filament and the context filaments, coronal loops and magnetic fields. **a-c**, AIA 304 Å (**a**) and 211 Å (**b**) images, and an HMI LOS magnetogram (**c**). The green rectangle in **a** denotes the FOV in Fig. 2a-c. FE and FS in **a** denote two nearby filaments. The ellipses in **b** and **c** enclose the footpoints of the loops L1. The yellow, blue and cyan dotted lines in **a** and **c** separately indicate the original filament and two newly reconnected filaments F1 and F2.

eastwards with a mean speed of $4.8 \pm 0.5 \text{ km s}^{-1}$. It then quickly erupts with a speed of $43.3 \pm 1 \text{ km s}^{-1}$ and an acceleration of $10.7 \pm 1 \text{ m s}^{-2}$, and is dispersed into many parallel dark threads L3 along the spine when viewed from above (see Fig. 2a and Supplementary Fig. 4). The other part of the filament erupts (marked by pink solid arrows in Supplementary Figs 1 and 3). Two flare ribbons (white arrows in Fig. 2b) and post-flare loops (see Supplementary Movies 1 and 4) appear underneath the erupting filament, in agreement with the classical flare models^{5,6}.

However, no increase of X-ray flux is observed. This indicates that no significant flare is associated with the filament eruption, as found in earlier observations of other related phenomena²⁵. This may be the reason why the following reconnection between the erupting filament and its nearby coronal loops can be clearly recognized: it is not simply dominated by the regular emission of flaring plasma. The southwestern part of the filament does not erupt owing to the constraint of the overlying coronal loops (see Fig. 1b). The eruption of the northeastern part of the filament is also observed by STEREO-B/EUVI simultaneously (see Supplementary Figs 1 and 3, and Supplementary Movie 2).

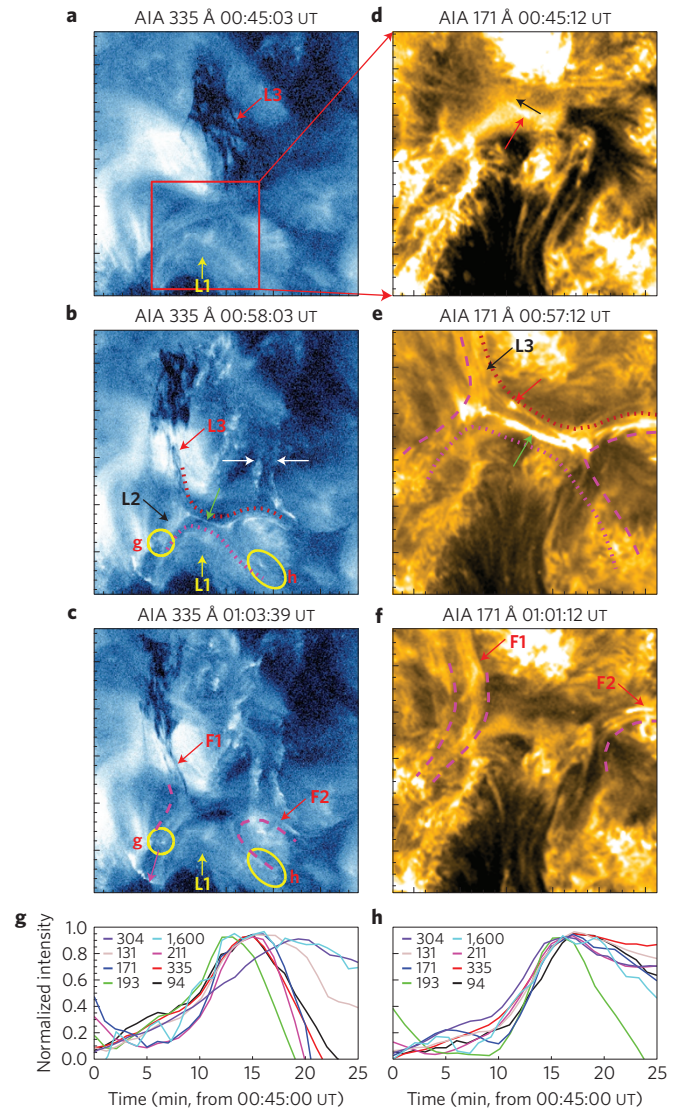


Figure 2 | Magnetic reconnection between the filament and the nearby coronal loops. **a-f**, AIA 335 Å (**a-c**) and 171 Å (**d-f**) images. **g,h**, Normalized light curves of AIA UV channels (wavelengths in Å given with the plots) in the yellow circles marked g and ellipses marked h in **b** and **c**. Thus, the light curves show the evolution of the footpoints of L2, F1 and F2. The red rectangle in **a** shows the FOV in **d-f**, and Fig. 4a,b. The red and pink dotted lines in **b** and **e** indicate the filament threads L3 and the loops L2, respectively. The pink dashed lines in **c,e** and **f** indicate F1 and F2. The green solid arrows in **b** and **e** mark the current sheets, the two white arrows in **b** mark two flare ribbons, the pink and black arrows in **c** and **d** indicate the propagation of the southern footpoints of F1 and a plasmoid, respectively, and the red solid arrows in **d** and **e** indicate the plasmoids.

During the eruption, the filament L3 encounters nearby coronal loops L2 and interacts with them, forming an X-type configuration with sheet-type and cusp-shaped structures at the interfaces (see the red and pink dotted lines in Fig. 2b). This X-type configuration is suggestive of magnetic reconnection³. The sheets in Fig. 2b (green arrow) indicate the positions of current sheets^{1-6,10}, which are the dissipation regions of magnetic energy during the reconnection process. The X-type loop structure is mainly observed in the channels of AIA that show hotter plasma, for example, at 335 Å and 211 Å. However, only the filament part of the X-structure is visible in the cooler channels of AIA, such as 193 Å ($\sim 1.5 \text{ MK}$), 171 Å ($\sim 0.9 \text{ MK}$), 131 Å ($\sim 0.6 \text{ MK}$), or 304 Å ($\sim 0.05 \text{ MK}$). Simultaneous brightenings in eight EUV and UV

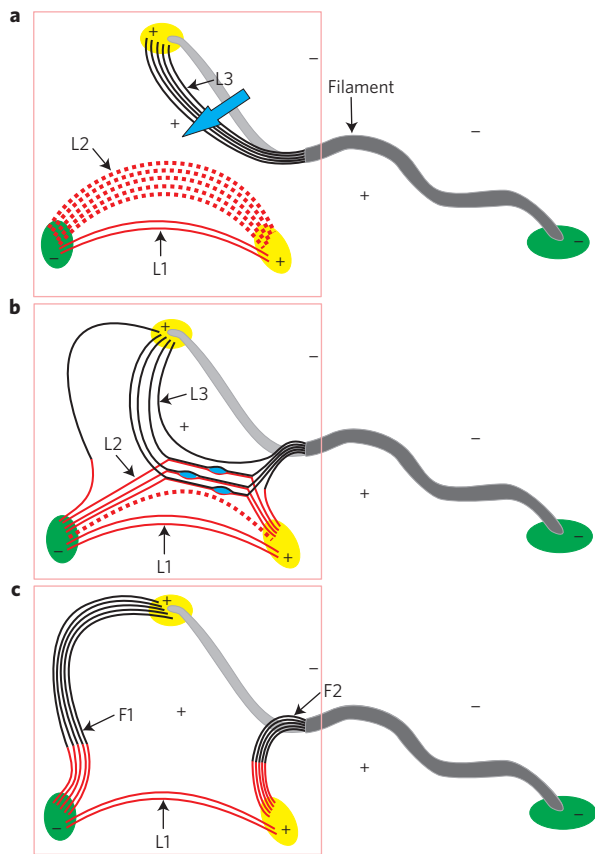


Figure 3 | Schematic diagrams of the magnetic reconnection. **a-c**, Magnetic field topology before **(a)**, during **(b)** and after **(c)** the magnetic reconnection. The yellow (plus) and green (minus) ellipses (signs) show the positive and negative magnetic fields. The grey thick lines indicate the filaments. The red, black and red-black lines denote the magnetic field lines. The cyan arrow in **a** shows the direction of eruption of the filament. The cyan ellipses in **b** indicate the plasmoids. L1 and L2 mark the hot loops observed in AIA higher-temperature channels (for example, 335 Å and 211 Å), L3 the initial filament threads, and F1 and F2 the newly reconnected filaments. The pink rectangles in **a-c** indicate the FOV in Fig. 2a-c.

channels of AIA at the loop footpoints (see the yellow circle labelled g and ellipse labelled h in Fig. 2b) are noticeable during the reconnection process (see Fig. 2g,h). They are heated by thermal conduction and/or non-thermal particles that are produced in the reconnection region^{1,2,4-6} and propagate along the newly reconnected magnetic field lines. The current sheets gradually diffuse and disappear. The northeastern part of the filament then reconnects to the eastern leg of the loops L2, forming a new filament F1, whereas the southwestern part reconnects to the western leg of L2, forming another new filament F2 (see Figs 1c and 2c). F1 forms orthogonally above the nearby east filament FE, which remains unchanged during the eruption and reconnection (see Supplementary Figs 1 and 3). This also applies to the nearby south filament FS. The southern footpoints of F1 show an apparent motion towards the southeast with a speed of $70 \pm 5 \text{ km s}^{-1}$ (see pink arrow in Fig. 2c and Supplementary Fig. 5). It indicates a continuing reconnection process. F1 stops erupting after the reconnection (see Supplementary Fig. 4 and Supplementary Movies 1, 2 and 4).

The southern (eastern) footpoints of F1 (F2) are the same as the eastern (western) footpoints of L2, see the yellow circles labelled g (ellipses labelled h) in Fig. 2b,c. This clearly indicates an interchange magnetic reconnection process between the magnetic field lines of the filament and the coronal loops.

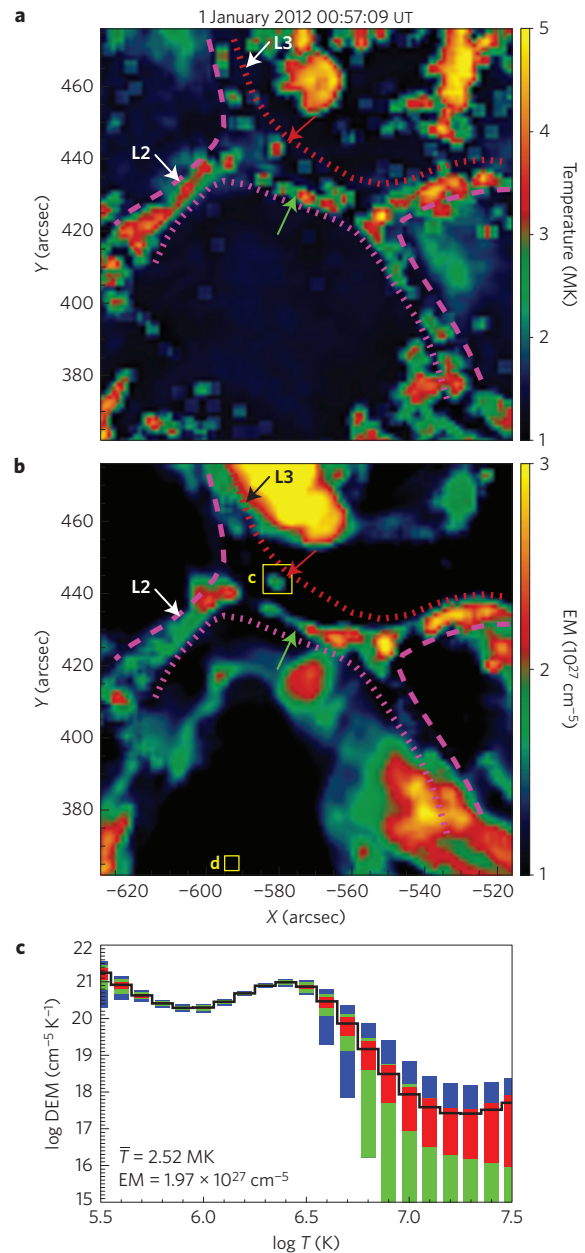


Figure 4 | Temperature and EM. **a,b**, Temperature **(a)** and EM **(b)** maps obtained using the DEM analysis method²⁶. **c**, DEM curve for a plasmoid region enclosed by the rectangle labelled c in **b**. The rectangle labelled d in **b** indicates the location where the background emission is measured. Similar to Fig. 2e, the dotted lines show the filament threads L3 and the loops L2, and the dashed lines the newly reconnected filaments. The green and red arrows mark a current sheet with plasmoids. The black curve in **c** is the best-fit DEM distribution. The red, green and blue rectangles in **c** separately represent the regions containing 50%, 51–80% and 81–95% of the Monte Carlo solutions.

The magnetic flux in the southern footpoint region of F1 is $(6 \pm 1) \times 10^{19} \text{ Mx}$ (see Supplementary Fig. 6). This flux has to equal the flux at the western footpoints of the loops L2 before the reconnection, and of the northern footpoints of F1 after the reconnection (see Fig. 2b,c and Supplementary Fig. 6). Thus, twice the flux of the southern footpoint, $(1.2 \pm 0.2) \times 10^{20} \text{ Mx}$, has been reconnected.

The reconnection of the filament and the apparent motion of the southern footpoints of F1 are also observed by EUVI 304 Å and 195 Å images (see Supplementary Fig. 3 and

Supplementary Movie 2). The filament material of the eastern part of F2 flows westwards into the unerupted filament part, and that of F1 flows down into its two footpoints. Both of the structures become invisible eventually in the cool lines (see Supplementary Movies 1, 2 and 4), as there is no cool filament material in them. It suggests that the newly reconnected magnetic field structures of both F1 and F2 cannot support dense filament material.

Because we observe no increase in X-rays, no significant flare is associated with the reconnection. A similar filament appears at the same position after the eruption and reconnection (see Supplementary Fig. 1). This indicates that the upper part, rather than the lower part, of the northern part of the filament erupts (see Fig. 3 and Supplementary Fig. 1). A narrow coronal mass ejection (CME) is observed associated with the filament eruption (see Supplementary Fig. 7). The main filament eruption is hence associated with a two-ribbon flare, post-flare loops, and a narrow CME, and causes the encounter and reconnection of the erupting filament L3 and the nearby coronal loops L2. However, the reconnection between L3 and L2 prevents L3 from erupting outwards (see Supplementary Fig. 4).

Although X-type structures indicative of magnetic reconnection have been reported before^{1,3}, here we can also investigate more details of the formation and evolution of plasmoids and current sheets. For this we refer also to Fig. 3, which gives an overall cartoon picture of what is happening in Fig. 2.

When the erupting filament L3 meets the neighbouring loops L2, a bright plasmoid appears and propagates northeastwards (red and black arrows in Fig. 2d). Also, a straight current sheet gradually brightens at the interface and later diminishes (see Supplementary Fig. 8 and Supplementary Movie 3). Subsequently, more filament threads reconnect with the pre-existing loops and form additional current sheets with propagating bright plasmoids (red and green solid arrows in Fig. 2e; see also Supplementary Figs 4, 8 and 9). After the current sheet disappears, the filament L3 connects all the way down to the southern footpoints of F1 (see Fig. 2f). In this process they move away from the reconnection region with speeds of about 40 km s⁻¹ to 170 km s⁻¹ (see Supplementary Fig. 8).

Investigating the temporal evolution, at least twelve individual current sheets are identified, moving southeastwards with velocities of about 35 km s⁻¹ to 120 km s⁻¹ (see Supplementary Fig. 8). Some of these current sheets merge (see Supplementary Figs 4 and 8). They last for about 11 ± 2 min, and have lengths of about 25'' to 41'', and widths of about 1.0'' to 1.6'' (see Supplementary Fig. 9).

Furthermore, many bright plasmoids appear within the current sheets and propagate bi-directionally along them, and then further along the filament or the loops (see Supplementary Fig. 8). They move with speeds of 100 km s⁻¹ to 300 km s⁻¹, have a widths of about 0.8'' to 1.7'', and are slightly ellipsoidal (see Supplementary Fig. 9). The plasmoids tend to move towards the erupting filament, as they mostly move northeastwards (see Supplementary Movie 3).

Details of the plasmoids in the reconnecting current sheets are clearly revealed by maps of temperature and emission measure (EM), which are obtained using a differential EM (DEM) analysis²⁶ of six AIA EUV channels at 94 Å, 335 Å, 211 Å, 193 Å, 171 Å and 131 Å (see Fig. 4 and Supplementary Movie 3). Consistent with the EUV observations, X-type structures, current sheets, and plasmoids are also identified in these temperature and EM maps shown in Fig. 4. The maps are cotemporal with the AIA 171 Å channel shown in Fig. 2e.

Inside the currents sheets (that is, the bright linear structures in Fig. 2e indicated by a green arrow), we see chains of enhanced temperature and EM (Fig. 4a,b). These are plasmoids, one of which is indicated by the solid red arrows in Fig. 4 and Fig. 2e. These plasmoids, and also current sheets, clearly have a multi-temperature structure, as they appear in AIA channels from 304 Å to 94 Å (see Supplementary Movie 3), which show different plasma

temperatures. The fairly broad DEM curve of the plasmoid shown in Fig. 4c also supports the multi-temperature distribution. Still the average (or mean) temperature in the plasmoid of 2.5 MK is higher than in the surroundings, underlining that the plasmoids not only have a broader distribution of temperatures, but that they are also hotter. Here the average temperature tends to be underestimated, as it is averaged over all the structures along the LOS.

Whereas there is little variation of the emission along the current sheets (Fig. 2e), there is a strong variation in temperature between the hot plasmoids and the cooler regions between them, which have lower than half the temperature of the plasmoids (Fig. 4a). However, overall the current sheets are significantly hotter than the filament threads measured before they reconnect, owing to the heating produced by reconnection.

The same applies for the EM. The density, $n = (EM R^{-1})^{0.5}$, of the current sheets can be estimated to range from $(3.5 \pm 0.5) \times 10^9 \text{ cm}^{-3}$ to $(5.0 \pm 0.5) \times 10^9 \text{ cm}^{-3}$, with the higher values found in the plasmoids. Here we assume that the depth R of a current sheet along the LOS is approximately equal to its width.

The spine of a filament consists of dense plasma concentrated around the centre of a longer magnetic flux tube^{16–20}, and so the disconnections and reconnections of the filament spine indicate a reconfiguration of magnetic field topology of the filament. Our observations represent a clear example of such reconnection and provide details of the process. In total, a magnetic flux of $(1.2 \pm 0.2) \times 10^{20} \text{ Mx}$ in the filament and the loops reconnects in about 11 min, resulting in a mean reconnection rate of $(2.0 \pm 0.7) \times 10^{17} \text{ Mx s}^{-1}$ (see Supplementary Fig. 6). This is an order of magnitude less than for strong X- or M-class flares²⁷, but is reasonable for reconfiguration in a non-flaring quiet Sun region, and that the reconnection flux here would correspond only to an A-class flare²⁸.

In the process there is a successive pile-up of magnetic field lines of the filament and the loops (see Fig. 3b), as in the flux-pile-up magnetic reconnection regime³. Thereafter, X-type structures and multiple current sheets gradually form (see Fig. 3b). The appearance of bright plasmoids in the current sheets (see Figs 2e, 3b and 4) suggests the presence of plasmoid instabilities^{10,29} during the reconnection. Magnetic reconnection releases and converts magnetic energy to kinetic energy^{1,4,10–14} and thermal energy^{3,4} (as well as particle acceleration). This is consistent with our observations, where the plasmoids are accelerated along the current sheets and show an enhanced temperature. As no associated X-ray increase is observed, only a small number of energetic particles may be produced during the reconnection in our case. We calculate the mean magnetic energy release rate by estimating the change of the magnetic energy in the reconnecting volume during the time of the reconnection event and find $(1.5 \pm 0.7) \times 10^{27} \text{ erg s}^{-1}$. Likewise we estimate the change of the thermal energy by integrating the internal energy over the volume and time of the reconnection, which gives $(4.0 \pm 3.1) \times 10^{26} \text{ erg s}^{-1}$. (Details on the magnetic and thermal energy can be found in Supplementary Fig. 6.) The comparison of the energy release rates shows that almost 30% of the magnetic energy is converted into thermal energy by magnetic reconnection.

Both the magnetic energy and the thermal energy release rates derived for the event studied here are less than those previously measured in X- and M-class flares³⁰. However, we gained an insight into the inner workings of the reconnection process that could not be achieved previously for larger flares, most probably because in those cases the plasmoids and other small-scale features in the reconnection process are outshone by the generally higher level of EUV and X-ray emission.

Data availability

Raw data is available from the Solar Dynamics Observatory (<http://sdo.gsfc.nasa.gov>) and Solar TERrestrial RELations

Observatory (<http://stereo.gsfc.nasa.gov>). Derived data supporting the findings of this study are available from the corresponding author on request.

Received 21 October 2015; accepted 13 April 2016;
published online 9 May 2016

References

- Priest, E. & Forbes, T. *Magnetic Reconnection* (Cambridge Univ. Press, 2000).
- Yamada, M., Kulsrud, R. & Ji, H. Magnetic reconnection. *Rev. Mod. Phys.* **82**, 603–664 (2013).
- Su, Y. *et al.* Imaging coronal magnetic-field reconnection in a solar flare. *Nature Phys.* **9**, 489–493 (2013).
- Aschwanden, M. Particle acceleration and kinematics in solar flares—a synthesis of recent observations and theoretical concepts (Invited Review). *Space Sci. Rev.* **101**, 1–227 (2002).
- Hirayama, T. Theoretical model of flares and prominences. I: Evaporating flare model. *Sol. Phys.* **34**, 323–338 (1974).
- Shibata, K. Evidence of magnetic reconnection in solar flares and a unified model of flares. *Astrophys. Spa. Sci.* **264**, 129–144 (1999).
- Tsuneta, S. *et al.* Observations of a solar flare at the limb with the YOHKOH soft X-ray telescope. *Publ. Astron. Soc. Jpn* **44**, L63–L69 (1992).
- Masuda, S., Kosugi, T., Hara, H., Tsuneta, S. & Ogawara, Y. A loop-top hard X-ray source in a compact solar flare as evidence for magnetic reconnection. *Nature* **371**, 495–497 (1994).
- Yokoyama, T., Akita, K., Morimoto, T., Inoue, K. & Newmark, J. Clear evidence of reconnection inflow of a solar flare. *Astrophys. J.* **546**, L69–L72 (2001).
- Takasao, S., Asai, A., Isobe, H. & Shibata, K. Simultaneous observation of reconnection inflow and outflow associated with the 2010 August 18 solar flare. *Astrophys. J.* **745**, L6 (2012).
- Wang, T., Sui, L. & Qiu, J. Direct observation of high-speed plasma outflows produced by magnetic reconnection in solar impulsive events. *Astrophys. J. Lett.* **661**, L207–L210 (2007).
- Tian, H. *et al.* Imaging and spectroscopic observations of magnetic reconnection and chromospheric evaporation in a solar flare. *Astrophys. J. Lett.* **797**, L14 (2014).
- McKenzie, D. & Hudson, H. X-ray observations of motions and structure above a solar flare arcade. *Astrophys. J.* **519**, L93–L96 (1999).
- Innes, D., McKenzie, D. & Wang, T. Observations of 1000 km s⁻¹ Doppler shifts in 10⁷ K solar flare supra-arcade. *Sol. Phys.* **217**, 267–279 (2003).
- Lin, J. *et al.* Direct observations of the magnetic reconnection site of an eruption on 2003 November 18. *Astrophys. J.* **622**, 1251–1264 (2005).
- Lin, Y. Filament thread-like structures and their small-amplitude oscillations. *Space Sci. Rev.* **158**, 237–266 (2011).
- Arregui, I. & Soler, R. Model comparison for the density structure along solar prominence threads. *Astron. Astrophys.* **578**, A130 (2015).
- Zhu, C., Alexander, D., Sun, X. & Daou, A. The role of interchange reconnection in facilitating a filament eruption. *Sol. Phys.* **289**, 4533–4543 (2014).
- Kumar, P., Manoharan, P. & Uddin, W. Evolution of solar magnetic field and associated multiwavelength phenomena: flare events on 2003 November 20. *Astrophys. J.* **710**, 1195–1204 (2010).
- van Driel-Gesztelyi, L. *et al.* Coronal magnetic reconnection driven by CME expansion—The 2011 June 7 event. *Astrophys. J.* **788**, 85 (2014).
- Lemen, J. *et al.* The Atmospheric Imaging Assembly (AIA) on the Solar Dynamics Observatory (SDO). *Sol. Phys.* **275**, 17–40 (2012).
- Schou, J. *et al.* Design and ground calibration of the Hemispheric and Magnetic Imager (HMI) instrument on the Solar Dynamics Observatory (SDO). *Sol. Phys.* **275**, 229–259 (2012).
- Pesnell, W., Thompson, B. & Chamberlin, P. The Solar Dynamics Observatory (SDO). *Sol. Phys.* **275**, 3–15 (2012).
- Howard, R. *et al.* Sun Earth Connection Coronal and Heliospheric Investigation (SECCHI). *Space Sci. Rev.* **136**, 67–115 (2008).
- McAllister, A., Dryer, M., McIntosh, P., Singer, H. & Weiss, L. A large polar crown coronal mass ejection and a “problem” geomagnetic storm: April 14–23 1994. *J. Geophys. Res.* **101**, 13497–13516 (1996).
- Cheng, X., Zhang, J., Saar, S. & Ding, M. Differential emission measure analysis of multiple structural components of coronal mass ejections in the inner corona. *Astrophys. J.* **761**, 62 (2012).
- Qiu, J., Wang, H., Cheng, C. & Gary, D. Magnetic reconnection and mass acceleration in flare-coronal mass ejection events. *Astrophys. J.* **604**, 900–905 (2004).
- Veronig, A. M. & Polanec, W. Magnetic reconnection rates and energy release in a confined X-class flare. *Sol. Phys.* **290**, 2923–2942 (2015).
- Bhattacharjee, A., Huang, Y., Yang, H. & Rogers, B. Fast reconnection in high-Lundquist-number plasmas due to the plasmoid instability. *Phys. Plasmas* **16**, 112102 (2009).
- Isobe, H., Takasaki, H. & Shibata, K. Measurement of the energy release rate and the reconnection rate in solar flares. *Astrophys. J.* **632**, 1184–1195 (2005).

Acknowledgements

The authors are indebted to the SDO and STEREO teams for providing the data. The work is supported by the National Natural Science Foundation of China (11533008, 11221063, 11303050, 11322329), CAS Project KJCX2-EW-T07, the Strategic Priority Research Program—The Emergence of Cosmological Structures of Chinese Academy of Sciences (No. XDB09000000), and a Young Researcher Grant of the National Astronomical Observatory, CAS. F.C. was supported by the International Max-Planck Research School (IMPRS) for Solar System Science at the University of Göttingen.

Author contributions

L.L. analysed the data, wrote the text and led the discussion. J.Z., H.P., E.P., H.C., L.G., F.C. and D.M. contributed to the data interpretation and helped to improve the manuscript.

Additional information

Supplementary information is available in the online version of the paper. Reprints and permissions information is available online at www.nature.com/reprints. Correspondence and requests for materials should be addressed to L.L.

Competing financial interests

The authors declare no competing financial interests.